

Criticality of the magnon-bound-state hierarchy for the quantum Ising chain with the long-range interactions

Yoshihiro Nishiyama

Department of Physics, Faculty of Science, Okayama University, Okayama 700-8530, Japan

Received: date / Revised version: date

Abstract. The quantum Ising chain with the interaction decaying as a power law $1/r^{1+\sigma}$ of the distance between spins r was investigated numerically. A particular attention was paid to the low-energy spectrum, namely, the single-magnon and two-magnon-bound-state masses, $m_{1,2}$, respectively, in the ordered phase. It is anticipated that for each σ , the scaled bound-state mass m_2/m_1 should take a universal constant (critical amplitude ratio) in the vicinity of the critical point. In this paper, we calculated the amplitude ratio m_2/m_1 with the exact diagonalization method, which yields the spectral information such as $m_{1,2}$ directly. As a result, we found that the scaled mass m_2/m_1 exhibits a non-monotonic dependence on σ ; that is, the bound state is stabilized by an intermediate value of σ . Such a feature is accordant with a recent observation based on the non-perturbative-renormalization-group method.

PACS. 75.10.Jm Quantized spin models – 05.70.Jk Critical point phenomena – 75.40.Mg Numerical simulation studies – 05.50.+q Lattice theory and statistics (Ising, Potts, etc.)

1 Introduction

The $O(N)$ -symmetric classical spin model with the long-range interactions has been investigated both theoretically [1, 2, 3, 4, 5, 6, 7, 8, 9, 10, 11, 12, 13, 14, 15, 16, 17] and experimentally [18, 19, 20, 21, 22, 23, 24, 25, 26, 27, 28]. A notable feature is that the power of the algebraic decay affects

the criticality of the order-disorder phase transition [1, 2]. Meanwhile, an extension to the quantum-mechanical version was made [29, 30, 31, 32, 33, 34]. As for the quantum Ising chain with the long-range interactions decaying as a power law $1/r^{1+\sigma}$ of the distance between spins r , there should appear three distinctive types of criticalities [31]; see Fig. 1. For $\sigma < 2/3$, the criticality belongs to the mean-field type; namely, the singularity is identical to that

of the four dimensional ($D = 4$) short-range classical Ising model. On the contrary, in $\sigma > 1.75$, the long-range interaction becomes irrelevant, and eventually, the criticality reduces to the $D = 2$ -short-range-classical-Ising universality class. In the intermediate regime $2/3 < \sigma < 1.75$, the singularity depends soothly on σ . Accordingly, the fractional dimensionality ranges within $2 < D < 4$ [7,8,9,31]. At both boundaries, particularly, at $\sigma = 1.75$, there emerge notorious logarithmic corrections [3,10,11,32], and the details as to the end-point singularities are controversial [4,5,6]. It has to be mentioned that the above-mentioned features are not a mere theoretical interest, because such an adjustable algebraic-decay rate σ is realized experimentally [19,20,23].

The criticality chart, Fig. 1, differs from that of the classical counterpart [1,2]. The difference comes from the fact that the real-space and imaginary-time directions are anisotropic for the quantum long-range criticality; the anisotropy is characterized by the dynamical critical exponent z [31], and accordingly, the set of scaling relations should be remedied. Aiming to elucidate the quantum-mechanical character of this problem, we shed light on the low-lying spectrum. In Fig. 2, we present a schematic drawing for the dispersion relations as to the low-lying elementary excitations in the ordered phase [35]. Here, the symbol $m_{1(2)}$ denotes the single-magnon (two-magnon-bound-state) mass. Above $2m_1$, there extends a continuum, and the series of bound states $m_{3,4,\dots}$ should be embedded within the continuum [36,37]. The bound-state hierarchy, namely, the scaled mass $m_{2,3,\dots}/m_1$, displays a universal character in

the vicinity of the critical point. As a matter of fact, according to the non-perturbative renormalization group [35], the scaled mass m_2/m_1 exhibits a non-monotonic dependence on D (fractional dimensionality); see Fig. 3. That is, an intermediate value of D stabilizes the bound state. Rather intriguingly, the hierarchy $m_{2,3,\dots}/m_1$ is relevant to the high-energy physics, that is, the gluon-bound-state spectrum (the so-called glueball spectrum) for the gauge field theory [38,39]. The universal values $m_{2,3}/m_1$ for the Ising model were explored extensively in this context [37].

In this paper, we investigate the scaled two-magnon-bound-state mass gap m_2/m_1 for the spin- $S = 1$ Ising chain with the long-range interactions (1). The extended spin $S = 1$ permits us to deal with the generalized (quadratic) interactions (D_s, γ_2) , which admit a clear signature for the bound-state mass (such as the plateau in Fig. 6 mentioned afterward) in the finite-size data. We employed the exact diagonalization method, which enables us to calculate the spectral properties such as $m_{1,2}$ directly without resorting to the inverse Laplace transformation; see Appendix B of Ref. [40]. In fairness, it has to be mentioned that recently, the dynamical properties for the long-range systems were studied with the exact diagonalization and the variational-matrix-product methods [41,42,43].

To be specific, the Hamiltonian for the quantum spin- $S = 1$ Ising chain with the long-range interactions is given by

$$\mathcal{H} = -\frac{1}{N} \sum_{i \neq j} J_{ij} S_i^z S_j^z + D_s \sum_i (S_i^z)^2$$

$$-\Gamma \sum_i \left(\frac{S_i^+}{\sqrt{2}} + \frac{\gamma_2}{2} (S_i^+)^2 + h.c. \right), \quad (1)$$

with the quantum spin- $S = 1$ operator $S_i^{\pm,z}$ placed at each one-dimensional lattice point, $i = 1, 2, \dots, L$. Here, the periodic boundary condition is imposed. The summation $\sum_{i \neq j}$ runs over all possible i - j pairs, and the symbol J_{ij} denotes the algebraically decaying interaction, $J_{ij} = 1/\sin(\pi|i-j|/L)^{1+\sigma}$, parameterized by σ . The Kac-normalization factor \mathcal{N} [41, 43] is given by $\mathcal{N} = L^{-1} \sum_{i \neq j} \sin(\pi|i-j|/L)^{-1-\sigma}$. The summation \sum_i runs over all spins $i = 1, 2, \dots, L$, and the single-ion anisotropy D_s is incorporated. The transverse magnetic field Γ , together with its quadratic variant γ_2 , drives the ferromagnetic state to the disordered phase. These redundant interaction parameters (D_s, γ_2) are tuned so as to attain a clear indication for the magnon bound state.

The rest of this paper is organized as follows. In the next section, we present the simulation results for the long-range Ising chain (1). The simulation algorithm is explained as well. In the last section, we address the summary and discussions.

2 Numerical results

In this section, we present the numerical results for the long-range quantum Ising chain (1). We employed the exact diagonalization method, which enables us to calculate the mass gaps $m_{1,2}$ directly. The numerical diagonalization was performed within the restricted Hilbert space specified by the quantum numbers such as the zero-momentum ($k = 0$) and the spin-inversion ($S_i^z \rightarrow -S_i^z$)

parity index, \pm . In a preliminary survey, we found that the single-magnon mass m_1 belongs to the sector

$$m_1 = E_1^+ - E_0^+, \quad (2)$$

with the ground-state (first-excited) energy E_0^+ (E_1^+) with the parity index $+$. Similarly, the two-magnon-bound-state mass m_2 is identified as either

$$m_2 = E_3^+ - E_0^+, \quad (3)$$

or

$$m_2 = E_2^- - E_0^+, \quad (4)$$

for small- and large- σ regimes, respectively; that is, the character of m_2 changes for respective regimes, as suggested by Fig. 3 [35].

2.1 Preliminary survey: Scaling behavior for the single-magnon mass m_1

As a preliminary survey, in this section, we investigate the scaling behavior for the single-magnon mass m_1 . To this end, we make use of the scaling theory developed in Ref. [31]. The interaction parameters are set to $(D_s, \gamma_2) = (0, 2)$ throughout this section.

In Fig. 4, we present the scaling plot, $(\Gamma - \Gamma_c)L^{1/\nu}L^z m_1$, with the critical point $\Gamma_c = 0.527$, the reciprocal correlation-length critical exponent $1/\nu = 0.84$, and the dynamical critical exponent $z = 0.60$ for the fixed $\sigma = 1.2$ and various system sizes, (+) $L = 18$, (\times) 20 , and (*) 22 . Here, the critical point $\Gamma_c = 0.527$ was extrapolated via the least-squares fit for the $L^{-1}-\Gamma_c(L)$ data with $L = 18, 20, 22$, and the approximative critical point $\Gamma_c(L)$ was

determined by the condition $\partial_{\Gamma} m_1|_{\Gamma=\Gamma_c(L)} = 0$ for each L . Similarly, the dynamical critical exponent $z = 0.60$ was determined via the least-squares fit for $(\frac{L+(L+2)}{2})^{-1} z(L, L+2)$ with $L = 16, 18, 20$, and the approximative dynamical critical exponent $z(L, L')$ is given by

$$z(L, L') = -\frac{\ln m_1(L)|_{\Gamma=\Gamma_c(L)} - \ln m_1(L')|_{\Gamma=\Gamma_c(L')}}{\ln L - \ln L'}. \quad (5)$$

As for the reciprocal correlation-length critical exponent $1/\nu = 0.84$, we made use of the existing value as addressed in Figs. 2 and 3 of Ref. [31].

From Fig. 4, we notice that the data collapse into a scaling curve satisfactorily. The single-magnon gap m_1 opens in the ordered phase $\Gamma - \Gamma_c < 0$. The gap m_1 sets a fundamental energy scale in the subsequent analyses in Sec. 2.2 and 2.3.

Carrying out similar analyses for various values of σ , we obtained the dynamical critical exponent z . The result is presented in Fig. 5. Here, as an indicator for the error, we accept the deviation between the different least-squares-fit analyses (abscissa scales), namely, the $(\frac{L+(L+2)}{2})^{-1}$ - and $(\frac{L+(L+2)}{2})^{-2}$ -based extrapolation schemes. In the large- σ side ($D \rightarrow 2$), the symmetry between the real-space and imaginary-time directions restores, and the dynamical critical exponent reflects the recovery, $z \rightarrow 1$. On the contrary, in the small- σ side, these spaces become asymmetric, $z < 1$. We stress that our simulation covers these two extreme cases with the interaction parameters fixed to $(D_s, \gamma_2) = (0, 2)$.

A few remarks are in order. First, the data at both boundaries, $\sigma = 2/3$ and 1.75, should suffer from corrections to scaling [3, 10, 11, 32]; particularly, the latter one at

$\sigma = 1.75$ has arisen controversies [4, 5, 6] as to the details of the end-point singularity. Because our main concern is the midst regime $\sigma \approx 1$, we do not pursue the details any further. Second, our data appear to obey an approximative formula [31]

$$z = \sigma/2. \quad (6)$$

Actually, as mentioned above, we obtained $z = 0.60$ for $\sigma = 1.2$; the result seems to agree with the formula, Eq. (6). The validity of Eq. (6) is not guaranteed for large σ [31] nonetheless. Last, the simulation was performed with the interaction parameters fixed to $(D_s, \gamma_2) = (0, 2)$. In the subsequent sections, we adjust the interaction parameters for the small- and large- σ regimes separately in order to attain a clear indication for m_2/m_1 .

2.2 Scaled two-magnon-bound-state mass m_2/m_1 :

Small- σ side

In this section, we analyze the scaled two-magnon-bound-state mass m_2/m_1 in the small- σ side. Here, the parameters are fixed to $(D_s, \gamma_2) = (-0.1, 2)$ so as to attain an appreciable plateau for m_2/m_1 .

In Fig. 6, we present the scaling plot, $(\Gamma - \Gamma_c)L^{1/\nu} m_2/m_1$, with the critical point $\Gamma_c = 0.568$ and the reciprocal correlation-length critical exponent $1/\nu = 0.73$ for $\sigma = 0.8$ and various system sizes, (+) $L = 18$, (\times) 20, and (\times) 22; here, the critical point $\Gamma_c = 0.568$ was determined with the same scheme as in Sec. 2.1, and the reciprocal critical exponent $1/\nu = 0.73$ is taken from Figs. 2 and 3 of Ref. [31]. We see a plateau with the height $m_2/m_1 \approx 1.9$

in the ordered phase $(\Gamma - \Gamma_c)L^{1/\nu} \approx -2 (< 0)$. We arrived at $m_2/m_1 = 1.895(10)$ via the least-squares fit for $L^{-1}m_2/m_1|_{\Gamma=\tilde{\Gamma}(L)}$ with $L = 18, 20, 22$; here, the location of the plateau (shallow valley) floor $\tilde{\Gamma}(L)$ satisfies $\partial_\Gamma(m_2/m_1)|_{\Gamma=\tilde{\Gamma}(L)} = 0$ for each L , and as an indicator for the error, we accept the deviation between the different least-squares-fit analyses (abscissa scales), namely, the L^{-1} - and L^{-2} -based extrapolation schemes. Carrying out similar analyses for various values of σ , we obtained the estimates as indicated by the symbol (+) in Fig. 7.

We address a number of remarks. First, for exceedingly large σ , the plateau width shrinks, and eventually, the plateau disappears. Such a feature suggests that the bound state (belonging to the (+) branch) is no longer supported by the long-range interactions with exceedingly large σ . Second, the shoulder around $(\Gamma - \Gamma_c)L^{1/\nu} \approx -2.5$ grows, as the system size L enlarges. Such a feature indicates the stability of the bound state. Last, around the boundary $\sigma = 2/3$, the simulation data suffer from the systematic errors, as noted in Ref. [32]. Because our concern is to survey the bound-state stabilization around $\sigma \approx 1$, we do not pursue the details any further.

2.3 Scaled two-magnon-bound-state mass m_2/m_1 :

Large- σ side

In this section, we analyze the scaled two-magnon-bound-state mass m_2/m_1 in the large- σ side. Here, the parameters are fixed to $(D_s, \gamma_2) = (0.2, 0.25)$.

In Fig. 8, we present the scaling plot, $(\Gamma - \Gamma_c)L^{1/\nu}m_2/m_1$, with the critical point $\Gamma_c = 0.913$ and the recip-

rocal correlation-length critical exponent $1/\nu = 0.88$ for $\sigma = 1.3$ and various system sizes, (+) $L = 18$, (\times) 20 , and (*) 22 ; here, the critical point $\Gamma_c = 0.913$ was determined with the same scheme as in Sec. 2.1, and the exponent $1/\nu = 0.88$ is taken from Figs. 2 and 3 of Ref. [31]. The hilltop height $m_2/m_1 \approx 0.85$ indicates the scaled bound-state mass. Via the least-squares fit for $L^{-1}m_2/m_1|_{\Gamma=\tilde{\Gamma}(L)}$ with $L = 18, 20, 22$, we obtained an estimate $m_2/m_1 = 1.879(17)$; here, the hilltop location $\tilde{\Gamma}(L)$ satisfies $\partial_\Gamma(m_2/m_1)|_{\Gamma=\tilde{\Gamma}(L)} = 0$ for each L , and as an indicator for the error, we accept the deviation between the different least-squares-fit analyses (abscissa scales), namely, the L^{-1} - and L^{-2} -based extrapolation schemes. Carrying out similar analyses for a variety of σ , we obtained a series of results as indicated by the symbol (\times) in Fig. 7.

We address a number of remarks. First, for exceedingly small σ , the hilltop location $\tilde{\Gamma}$ shifts into the disordered phase, and the branch terminates. Last, the data around the boundary $\sigma = 1.75$ should suffer from the systematic errors [3, 10, 11].

2.4 Comparison with the preceeding results via the $\sigma \leftrightarrow D$ relation [8]

In this section, we make a comparison with the preceding results such as the fixed- $D = 3$ analyses [37, 44, 45] and the non-perturbative renormalization group for ${}^\forall D$ [35]. In order to establish a relationship between them and ours, we rely on the $\sigma \leftrightarrow D$ relation [8, 31]

$$D = 2/\sigma + 1, \quad (7)$$

which is validated for small- σ (large- D) regime; more sophisticated formulas [31] do not take such a closed expression.

The overall features of Fig. 7 and 3 [35] resemble each other; actually, the magnon bound state is stabilized by an intermediate value of σ and D , respectively. Such stabilization of the bound-state mass is captured by neither mean-field theory ($D = 4$) nor free-fermion picture ($D = 2$).

A number of remarks are in order. First, we consider the case $D = 3$. This case corresponds to $\sigma = 1$ according to the $\sigma \leftrightarrow D$ relation (7). Our result indicates $m_2/m_1 = 1.845(10)$ at $\sigma = 1$ (along side of the (\times) branch). On the one hand, by means of the Monte Carlo [37], series expansion [44], and exact diagonalization [45] methods, the estimates, $m_2/m_1 = 1.83(3)$, 1.81 , and $1.84(1)$, respectively, were obtained for the fixed- $D = 3$ systems. Additionally, the $\forall D$ non-perturbative-renormalization-group method yields $m_2/m_1 = 1.82(2)$ at $D = 3$ [35]. Our result appears to be consistent with these preceding elaborated analyses. According to the super-universality idea, the long- and the short-range models are related with a relation such as Eq. (7) at least for the large- D side [8]. Our data suggest that down to $D = 3$, the relationship is retained even for the spectral properties such as m_2/m_1 . Second, we turn to considering the case, $D \neq 3$. The non-perturbative renormalization group [35] predicts that the minimum point locates around $D = 2.7$ - 2.8 , where the scaled mass takes $m_2/m_1 = 1.65$ - 1.7 . On the contrary, our result resolves neither appreciable deviation of the minimum point from $D = 3$ ($\sigma = 1$) nor notable drop of m_2/m_1 in the small- D

side. The discrepancy may be attributed to the breakdown of a naive $\sigma \leftrightarrow D$ correspondence for such small- D regime. Last, we provide a brief overview on the $\sigma \leftrightarrow D$ relation (7). In the course of the studies [7, 8, 11], the concept of the $\sigma \leftrightarrow D$ relation has been developed. As for the quantum-mechanical system, there was reported a refined formula $D = (2 - \eta_{SR}(D)) \frac{1+z(\sigma)}{\sigma}$ [31]. Here, the symbol $\eta_{SR}(D)$ denotes the critical exponent for the short-range model in D dimensions. The explicit expressions for $\eta_{SR}(D)$ and $z(\sigma)$ are unclear. We resort to the approximate relations, $\eta_{SR} = 0$ and $z = \sigma/2$ (6), which are validated in the large- D (small- σ) regime [31]. As mentioned above, these formulas lead to the closed expression, Eq. (7).

3 Summary and discussions

The quantum spin- $S = 1$ Ising chain with the long-range interactions (1) was investigated numerically. So far, as for the classical counterpart, a thorough investigation has been made. Aiming to elucidate the quantum nature of this problem, we shed light on its low-energy spectrum, namely, the single-magnon and bound-state masses, $m_{1,2}$, respectively, in the ordered phase. For that purpose, we employed the exact diagonalization method, which enables us to calculate $m_{1,2}$ directly. As a result, we obtained the σ -dependent scaled bound-state mass, m_2/m_1 , for various values of the algebraically-fall-off exponent, σ .

Thereby, based on the $\sigma \leftrightarrow D$ relation (7), we obtained the result $m_2/m_1 = 1.845(10)$ for $D = 3$. Our result is to be compared with the preceding results, $m_2/m_1 = 1.83(3)$, 1.81 , $1.84(1)$, and $1.82(2)$ via the Monte Carlo

Fig. 1. The quantum Ising chain with the algebraically decaying interactions $\propto 1/|i-j|^{1+\sigma}$, Eq. (1), exhibits the order-disorder phase transition. The criticality (universality class) depends on the fall-off exponent σ , and the singularity is classified into three regimes [31]. For small $\sigma < 2/3$, the phase transition belongs to the mean-field type, namely, the $D = 4$ -classical-Ising universality class. For large $\sigma > 1.75$, on the contrary, it is identical to that of the $D = 2$ Ising model. In the intermediate regime $2/3 < \sigma < 1.75$, the singularity is controlled by σ continuously, and correspondingly, the fractional dimensionality changes within $2 < D < 4$ [8]. At the boundaries, particularly, at $\sigma = 1.75$, there appear notorious logarithmic corrections [3, 10, 11, 32].

[37], series expansion [44], exact diagonalization [45], and non-perturbative-renormalization-group [35] methods, respectively. Hence, it is indicated that down to $D = 3$, the validity of super-universality [8] is retained even for the spectral properties such as m_2/m_1 . The magnon-bound-state hierarchy is relevant to the glueball spectrum for the gauge field theory [38, 39]. It would be intriguing that such high-energy phenomenology is explored [46] for the magnetic materials [36] with finely-tunable [19, 20, 23] long-range interactions.

References

1. M. E. Fisher, S.-k. Ma, and B. G. Nickel, Phys. Rev. Lett. **29** (1972) 917.
2. J. Sak, Phys. Rev. B **8** (1973) 281.
3. E. Luijten and H. W. J. Blöte, Phys. Rev. Lett. **89** (2002) 025703.
4. M. Picco, arXiv:1207.1018.
5. T. Blanchard, M. Picco, and M. A. Rajabpour, Europhys. Lett. **101** (2013) 56003.
6. P. Grassberger, J. Stat. Phys. **153** (2013) 289.
7. G. Gori, M. Michelangeli, N. Defenu, and A. Trombettoni, Phys. Rev. E **96** (2017) 012108.
8. M. C. Angelini, G. Parisi, and F. Ricci-Tersenghi, Phys. Rev. E **89** (2014) 062120.

Fig. 2. A schematic drawing for the low-lying spectrum of the quantum Ising model in the ordered phase is presented. At the zone center $k = 0$, there open the single-magnon- and two-magnon-bound-state-mass gaps, $m_{1,2}$, respectively. Above $2m_2$, there extends a continuum, and the magnon-bound-state hierarchy $m_{3,4,\dots}$ should be embedded within the continuum. The bound state is stabilized around $D \approx 3$, as shown in Fig. 3.

Fig. 3. According to the non-perturbative renormalization-group analysis [35], the scaled bound-state mass m_2/m_1 exhibits a non-monotonic dependence on the fractional dimensionality D of the short-range *classical* Ising model, namely, the $(D - 1)$ -dimensional *quantum* Ising model with the short-range interactions. As a reference, a plot $m_2/m_1 = 1.82(2)$ at $D = 3$ [35], which is of particular importance, is indicated.

9. J. S. Joyce, Phys. Rev. **146** (1966) 349.
10. E. Brezin, G. Parisi, and F. Ricci-Tersenghi, J. Stat. Phys. **157** (2014) 855.
11. N. Defenu, A. Trombettoni, and A. Codello, Phys Rev. E **92** (2015) 052113.
12. N. Defenu, A. Trombettoni, and S. Ruffo, Phys. Rev. B **94** (2016) 224411.
13. R. Goll and P. Kopietz, arXiv:1804.04150.
14. E. Flores-Sola, M. Weigel, R. Kenna, and B. Berche, Eur. Phys. J. Special Topics **226** (2017) 581.
15. T. Horita, H. Suwa, and S. Todo, Phys. Rev. E **95** (2017) 012143.
16. G. Sun, Phys. Rev. A **96** (2017) 043621.

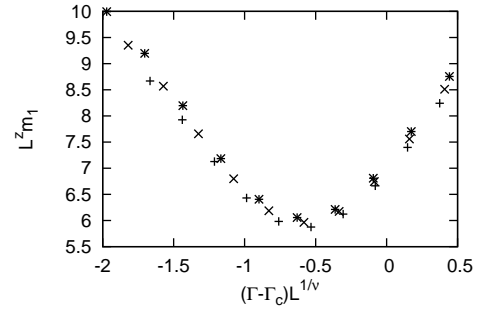


Fig. 4. The scaling plot, $(\Gamma - \Gamma_c)L^{1/\nu} - L^z m_1$, with the critical point $\Gamma_c = 0.527$, the reciprocal correlation-length critical exponent $1/\nu = 0.84$, and the dynamical critical exponent $z = 0.60$ is presented for $\sigma = 1.2$ and various system sizes, $(+)$ $L = 18$, (\times) 20 , and $(*)$ 22 ; see text for details. Here, the interaction parameters are set to $(D_s, \gamma_2) = (0, 2)$.

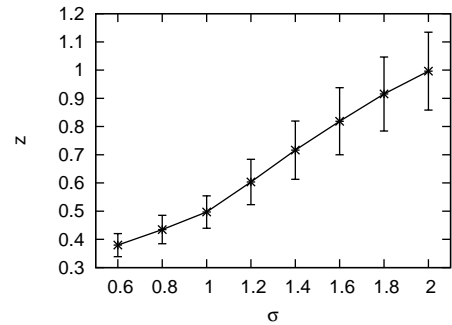


Fig. 5. The dynamical critical exponent z is presented for various values of the algebraically-fall-off exponent σ ; see text for details. Here, the interaction parameters are set to $(D_s, \gamma_2) = (0, 2)$.

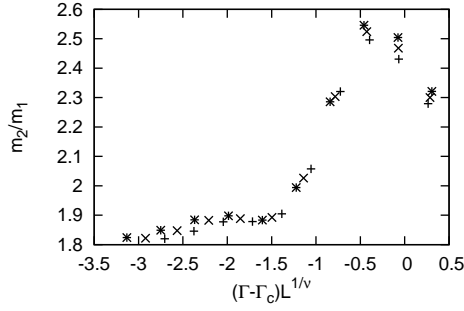


Fig. 6. The scaling plot, $(\Gamma - \Gamma_c)L^{1/\nu} - m_2/m_1$, with the critical point $\Gamma_c = 0.568$ and the reciprocal correlation-length critical exponent $1/\nu = 0.73$ is presented for $\sigma = 0.8$ and various system sizes, (+) $L = 18$, (\times) 20 , and (*) 22 . Here, the interaction parameters are set to $(D_s, \gamma_2) = (-0.1, 2)$. The height of the plateau $m_2/m_1 \approx 1.9$ indicates an amplitude ratio; the extrapolated one is plotted in Fig. 7. As the system size enlarges, the shoulder around $(\Gamma - \Gamma_c)L^{1/\nu} \approx -2.5$ extends leftward, suggesting the stabilization of the bound state in the thermodynamic limit.

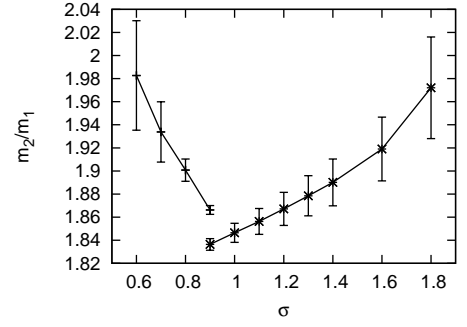


Fig. 7. The scaled bound-state mass m_2/m_1 is presented for various values of the algebraically-fall-off exponent σ . The plots, (+) and (\times), are determined in Sec. 2.2 and 2.3, respectively.

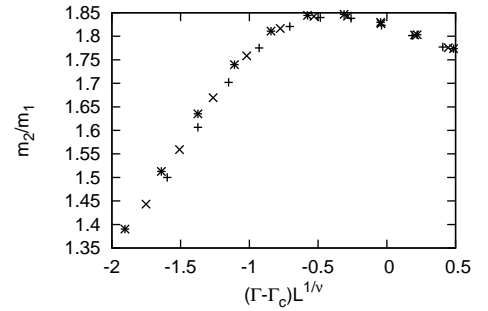


Fig. 8. The scaling plot, $(\Gamma - \Gamma_c)L^{1/\nu} - m_2/m_1$, with the critical point $\Gamma_c = 0.913$ and the reciprocal correlation-length critical exponent $1/\nu = 0.88$ is presented for $\sigma = 1.3$ and various system sizes, (+) $L = 18$, (\times) 20 , and (*) 22 . Here, the interaction parameters are set to $(D_s, \gamma_2) = (0.2, 0.25)$. The hilltop height $m_2/m_1 \approx 1.85$ indicates an amplitude ratio; the extrapolated one is plotted in Fig. 7.

17. S. Humeniuk, Phys. Rev. B **93** (2016) 104412.
18. W. Wu, B. Ellman, T. F. Rosenbaum, G. Aeppli, and D. H. Reich, Phys. Rev. Lett. **67** (1991) 2076.
19. J. W. Britton, B. C. Sawyer, A. C. Keith, C.-C. Joseph Wang, J. K. Freericks, H. Uys, M. J. Biercuk, J. J. Bollinger, Nature **484** (2012) 489.
20. R. Islam, C. Senko, W.C. Cambell, S. Korenblit, J. Smith, A. Lee, E. E. Edwards, C.-C. J. Wang, J. K. Freericks, and C. Monroe, Science **340** (2013) 583.
21. J. G. Bohnet, B. C. Sawyer, J. W. Britton, M. L. Wall, A. M. Rey, M. Foss-Feig, and J. J. Bollinger, Science **352** (2016) 1297.

22. J. Zhang, G. Pagano, P. W. Hess, A. Kyprianidis, P. Becker, H. Kaplan, A. V. Gorshkov, Z.-X. Gong, and C. Monroe, *Nature* **551** (2017) 601.
23. P. Richerme, Z.-X. Gong, A. Lee, C. Senko, J. Smith, M. Foss-Feig, S. Michalakakis, A.V. Gorshkov, and C. Monroe, *Nature* **511** (2014) 198.
24. P. Jurcevic, B.P. Lanyon, P. Hauke, C. Hempel, P. Zoller, R. Blatt, and C.F. Roos, *Nature* **511** (2014) 202.
25. A. de Paz, A. Sharma, A. Chotia, E. Maréchal, J.H. Huckans, P. Pedri, L. Santos, O. Gorceix, L. Vernac, and B. Laburthe-Tolra, *Phys. Rev. Lett.* **111** (2013) 185305.
26. A. Browaeys, D. Barredo, and T. Lahaye, *J. Phys. B* **49** (2016) 152001.
27. S.A. Moses, J.P. Covey, M.T. Miecnikowski, D.S. Jin, and J. Ye, *Nat. Phys.* **13** (2017) 13.
28. P. Schauß, M. Cheneau, M. Endres, T. Fukuhara, S. Hild, A. Omran, T. Pohl, C. Gross, S. Kuhr, and I. Bloch, *Nature* **491** (2012) 87.
29. N. Laflorencie, I. Affleck, and M. Berciu, *J. Stat. Mech.: Theory and Experiment*, P12001 (2005).
30. A. Dutta and J. K. Bhattacharjee, *Phys. Rev. B* **64** (2001) 184106.
31. N. Defenu, A. Trombettoni, and S. Ruffo, *Phys. Rev. B* **96** (2017) 104432.
32. S. Fey and K. P. Schmidt, *Phys. Rev. B* **94** (2016) 075156.
33. A. W. Sandvik, *Phys. Rev. Lett.* **104** (2010) 137204.
34. T. Koffel, M. Lewenstein, and L. Tagliacozzo, *Phys. Rev. Lett.* **109** (2012) 267203.
35. F. Rose, F. Benitez, F. Léonard, and B. Delamotte, *Phys. Rev. D* **93** (2016) 125018.
36. R. Coldea, D. A. Tennant, E. M. Wheeler, E. Wawrzynska, D. Prabhakaran, M. Telling, K. Habicht, P. Smeibidl, and K. Kiefer, *Science* **327** (2010) 177.
37. M. Caselle, M. Hasenbusch, P. Provero, *Nucl. Phys. B* **556** (1999) 575.
38. V. Agostini, G. Carlino, M. Caselle, and M. Hasenbusch, *Nucl. Phys. B* **484** (1997) 331.
39. R. Fiore, A. Papa, and P. Provero, *Phys. Rev. D* **67** (2003) 114508.
40. S. Gazit, D. Podolsky, A. Auerbach, and D. P. Arovas, *Phys. Rev. B* **88** (2013) 235108.
41. I. Homrighausen, N. O. Abeling, V. Zauner-Stauber, J. C. Halimeh, *Phys. Rev. B* **96** (2017) 104436.
42. I. Frérot, P. Naldesi, T. Roscilde, *Phys. Rev. Lett.* **120** (2018) 050401.
43. L. Vanderstraeten, M. Van Damme, H. P. Büchler, F. Verstraete, *arXiv:1801.00769*.
44. S. Dusuel, M. Kamfor, K. P. Schmidt, R. Thomale, and J. Vidal, *Phys. Rev. B* **81** (2010) 064412.
45. Y. Nishiyama, *Physica A* **413** (2014) 577.
46. B. Svetitsky and L. G. Yaffe, *Nucl. Phys. B* **210** (1982) 423.